مجلة إتحاد الجامعات العربية

An Investigation of Hydraulic and Thermal Performance of Metal Foam Filter

Ihsan Y. Hussain
Professor
Mohammad Y. Shaker
Mech. Engr. Dept
College of Engineering
University of Baghdad \Iraq

Abstract

Hydraulic and thermal performance of metal foam filter were investigated numerically and experimentally in the present work for clean and dusty air in a, copper foam filter. Two pore densities of copper foams are used, 10 PPI with average pore diameter 905.7 μm with porosity (90%) and 40PPI with average pore diameter 568.6 μm with porosity (89%). Copper foam filter exposed to different air inlet constant temperature of clean and dusty air for different values of pore Reynolds number (Rep) which are (119.1, 168, 218, 306.8, and 356.7) for 10 Pore Per Inch (PPI) and are (73.8, 104.21, 135.21, 190.3, and 221.3) for (40PPI). The samples are tested in a wind tunnel and exposed to a clean and dusty air at different inlet constant temperatures (29.7˚C, 40˚C, 50˚C, 60˚C, 65˚C) as a thermal boundary condition. The tests included the measurements of pressure and temperature distributions through the metal foam samples. In the numerical solution, the effect of temperature and pressure are studied and discussed by using a CFD Package Comsol Multiphysics 4.3b by solving three dimensional [continuity, momentum (Forchheimer′s equation) and energy] equations. The numerical investigation covered all the cases of the experimental work. The results show that the absolute pressure decreased along the flow direction, and increased with the increase of pore Reynolds number. No effect of temperature was noticed on the results. For clean air the results show that the pressure drop (ΔP) of 40PPI is higher by (57.8%) than that for the 10PPI. For dusty air, the results show that the absolute pressure increased with increasing dust concentration (C) or dust density (N= 2, 4, 6 & 8), and the pressure drop through copper foam filter with 40PPI is higher by (58.09%) than that for the 10PPI, and the pressure drop for dusty air at dust density (N= 2 & 4) is higher by (33%) than the clean air at same conditions. Comparison between the present experimental and numerical results shows a similar behavior with a minimum and maximum deviation of 1-5%. The present experimental and numerical results also have been compared with available previous studies for pressure (P) with x-axis and pressure gradiant (ΔP/L) with velocity, and showed a good agreement.

Key Words: Metal Foam Filter, Clean and Dusty Air, Numerical and Experimental Study

1-Introduction

Cellular (porous) metals and metallic foams are metals with pores deliberately integrated in their structure, where these structures are generaly having large volume of

porosities. Metal foams have very high porosity (as high as 99%), very high surface area to volume ratio (up to 5000m^2/m^3), tortuous and irregular (randomly oriented cells) shapes, flow passages that has a solid matrix made of metal with empty or fluid filled voids space. The porosity is defined as the ratio of total voids (pores) volume to cumulative volume occupied by the solid matrix and pore space

($\varepsilon = V_{pore} / V_{total}$). Two types of metal foams are found, closed cell metal foams have voids not connected via open channels and open cell metal foams have interconnected voids with each other. The open type is used for heat exchangers, filters systems, chemical reactors, catalytic converters, compact electronics cooling, energy absorption, geothermal applications and so on. The number of pores per linear inch (PPI) currently ranges from 5 to 100, obviously, each type of foam lends itself to suitable applications. Mother metals include aluminum and its alloys, nickel and its alloys, copper, titanium alloy, steel, lead and its alloys, silver, gold, etc. Numerous studies exist in the literature that investigates thermal (heat transfer rate, thermal resistance, etc.) and hydraulic (pressure drop, drag form coefficient, permeability)

characteristics of metal foam. Kopanidis et al. [1] presented three dimensional model at the pore scale level for the flow and heat transfer of open cell metal foam with high porosity of two pore densities (10 PPI & 40 PPI). By solving of the Navier–Stokes and energy equations under various flow and temperature conditions, the authors obtained the conjugate flow and temperature fields. Macroscopic characteristics (heat transfer coefficient & pressure drop) were investigated and the influence of entrance effects on it. Model validation was conducted against macroscopic parameters. The results are found in reasonable agreement with the experimental measurements. Lee et al. [2] developed a mathematical model for the filtration process and soot regeneration in a nickel metal foam filter to study the radial type performance of a metal foam diesel particulate filter (DPF). The pores diameter of the open cell metal foams in the DPF are increased from 580 µm to 800 µm. The study led to decreasing of the filtration efficiency from 90% to 50%, decreasing of the pressure drop from 380 mbar to 20 mbar and DPF with a large pore diameter of metal foam is effective in using the volume of material with a small pressure drop. Anurag and Singh [3] studied the effect of dusty viscous fluid on unsteady laminar free convection flow through porous medium along a moving porous hot vertical plate in the presence of heat source and thermal diffusion with mass transfer. The governing equations of motion were solved by finite difference technique. The numerical results were presented graphically for

different values of the parameters affecting onto the problem on the velocity profiles of dusty fluid, dust particles, temperature, concentration profile and skin friction profile. Andrea et al. [4] numerically analysis presented for air flow through four different porosity ERG copper foams with high porosity and different pore densities (5, 10, 20, &40 PPI), and almost with the same relative density (6.4-6.6% solid fraction). Copper foams were scanned by a commercial micro computed tomography scanner with a 20µm as a resolution. Fluid flow simulations were performed using the package program (ANSYS Fluent) to simulate the fluid flow through the pore space of the copper foams. Further, the pressure gradient increases as the PPI increases. The outcomes of X-Ray Micro Computed Tomography (µ-CT) based CFD computations and these results are compared against previously experimental measurement of pressure drop with same samples. A good agreement was obtained between numerical and experimental results. Simone et al. [5] experimentally investigated the air forced convection through five electrically heated copper foam samples with different PPI (5, 10, 20, & 40PPI) and different high porosities (90.5%-93.4%). The experiments are conducted by varying the air mass flow rate between (0.006 & 0.012 kg/s), and three heat fluxes 25, 32.5 and 40 kW/m^2. The collected heat transfer and pressure drop data were analyzed to obtain the global heat transfer coefficient, the normalized mean wall temperature, the pressure gradient, drag coefficient, inertia coefficient and permeability, the heat transfer coefficient does not based on the imposed heat flux and it increases with the air mass flow rate. The pressure drops increase with increased pore density (PPI). Koltsakis et al. [6] experimentally and CFD investigated a new porous material based on the Incofoam high temperature and Nikle-based super alloy foam were used in a particulate filter concept with different structures of foam and variable pore characteristics. Pressure drop, the filtration characteristics and performance of the regeneration were tested and studied for different filter configurations depending on the experimental data and modeling. Pressure drop and flow behavior with exhaust gas and air and the filtration efficiency measurements were covered by the experimental testing. These parameters were a function of the regeneration rate measurements and size of particle. By employing the CFD studies, the macroscopic structure of metal foams filter was improved. The results proved that the filtration efficiency of the foam filter can be reached 90% at an acceptably low pressure drop. The regeneration rates in the case of the catalyst-coated foams at low temperatures are very high. Rémy et al. [7] carried out the experiments of the filtration process for the particles generated in fluidized bed gasification

by utilizing nickel–chromium foams. In generally, the metal foams have inherent properties make it very suitable for use in structures because of the high temperature resistance, corrosion resistance and strength. The structurally characterized for the metal foams are obtained by (topology of cell, relative density, very high porosity ($\varepsilon = 0.95$) and cell size. In hot gas filtration the specific area ratio required low pressure drop and high temperature resistance as an essential characteristics. The effect of different experimental operating parameters such as heating time, foam thickness and temperature were investigated. The pressure drop was calculated during filtration process. A good agreement is obtained between the experimental and numerical simulation results. Metal foams were effective for the removal of particles contained in hot gases. Kashif et al. [8] analyzed the thermal-hydraulic performance of the open-cell aluminum foams heat exchangers, aluminum foams are used as a highly consolidated replacement for traditional fins in brazed aluminum heat exchangers. By a closed-loop wind tunnel, the experiments were conducted to obtained the heat transfer rates and the pressure drop. The impacts of bonding method, different porosity, condensation, base metal and frost were observed. Metal foams with small pores diameter caused an increase in pressure gradient (not preferred) and higher heat transfer rate. To reduce the pressure drop in metal foam, fin depth can be altered. Metal foams were found to carry out much better thermal-hydraulic performance compared to another designs using plain or louver fins with much larger coefficients of heat transfer. Flow characteristics (permeability & inertia coefficients) were calculated and compared with the reported data. Developing the model was related to foam characteristics, flow conditions,

and the pressure drop and heat transfer depending on experimental results. By using a Reynolds number based on hydraulic diameter, curves fits for the friction factor and for Colburn *j* factor based on pore diameter, were developed with reasonable engineering accuracy.

NUMERICAL SIMULATION:

The geometry of the present work is shown in **Figure1**. The system geometry is a three dimensional with Cartesian coordinates, where the x-direction represents the flow direction. The system geometry consists of a box (which represents the flow tunnel) and this box contains a copper foams saturated with clean air and dusty air. The box dimensions are L_1=150mm, W_1=100mm and H_1=100mm. This box is filled with copper foams with different pore densities (10PPI and 40PPI).

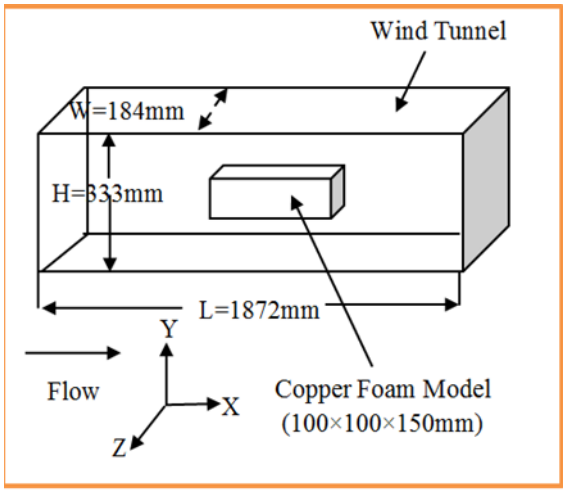

Figure (1): Model Geometry

At the macro-scale simulations and in order to analyze or to describe the airflow and laminar forced convection characteristics in a copper foams filter under clean and dusty air effects with dust ratio values (density number N) of (2, 4, 6 and 8), a solution of a differential forms of Forchheimer's (momentum equation) and energy equations are required. A numerical solution of the flow field (hydraulic performance) and heat transfer process and temperature distribution (thermal performance) in copper foams filter, using governing partial differential equations which are based on the conservation of mass, momentum and energy equations (with boundary conditions) was made numerically using Comsol Multiphysics 4.3b after describing the mesh model using the appropriate discretization. The mesh conventions-cell type tetrahedral / hybrid in 3D, see figure (2), was used for mesh generation to approximate precisely the geometry interfaces. Complete mesh consists of 68607 domain elements, 6656 boundary elements, and 268 edge elements (fine mesh), number of degrees of freedom solved (DOFs) for: 227381 (plus 2500 internal DOFs) in order to find more accurate results.

Governing Equations

Continuity Equation

The conservation of mass for three-dimensional averaged flow through a porous medium is expressed by the following continuity equation Nield and Bejan [9];

$$\varepsilon \frac{\partial \rho_f}{\partial t} + \nabla.\left(\rho_f \vec{V}\right) = 0 \quad \text{..... (1)}$$

The saturated fluid density (ρ_f) is constant except for the buoyancy force, which results in;

$$\nabla.\vec{V} = 0 \quad \text{.....(2)}$$

or

$$\frac{\partial u}{\partial x} + \frac{\partial v}{\partial y} + \frac{\partial w}{\partial z} = 0 \quad \text{..... (3)}$$

Momentum Equation

Conservation of momentum using Brinkman – Forchheimer extended Darcy Model (non darcian effects) taking the effect of viscous and inertial forces into account as well as the porosity variation near the walls. The macroscopic governing equations are derived according to the volume averaging technique Whitaker [10].

The momentum equation for a fluid saturated metal foams can be written as:

$$\frac{\rho_f}{\varepsilon}\left[\nabla\left(\frac{V.V}{\varepsilon}\right)\right] = -\nabla p + \mu_e \nabla^2 V - \left[\frac{\mu V}{K} - \frac{\rho_f C_F}{\sqrt{K}} V|\bar{V}|\right] \quad \text{..... (4)}$$

C_F is the Forchheimer's coefficient, and is the geometric function (form drag) can be represented as in Ergun [11] and Vafai [12] (Egrun's correlation);

$$K = \frac{\varepsilon^3 d^2 p}{150(1-\varepsilon)^2} \text{ and } C_F = \frac{1.75}{\sqrt{150\,\varepsilon^3}} \text{ ...(5)}$$

Where;

d_p: Average pore diameter (mm)

In case the dusty air passing through the copper foams filter in order to calculate the dust concentration effects on the hydraulic and thermal performance of copper foams air filter Shyamanta [13], and AL-Sumaily et al. [14] and Salman [15], below the govering equation of the dust concentration;

$$C = \frac{N}{Q} \quad \text{..... (6)}$$

Where;

C= Dust particle concentration (size of dust particles 75 µm) (g/m^3) N= Dust density (g/min)

Q= Discharge of air (m^3/min)

Energy Conservation Equation

This work is mainly concerned with the transport of heat and temperatures distribution, in addition to air flow, through copper foams filter. There is a large number of applications, particularly in mechanical engineering, where the thermal aspect is fundamental: solidification of binary mixtures, dehumidification, insulation, filtration and heat pipes Kaviany [16]. In all these cases the temperatures distribution inside the medium can be recovered from the solution of energy conservation equation, coupled to the momentum conservation and continuity equations. The macroscopic energy equation for a saturated metal foams, derived using the volume averaging procedure, assuming local thermal equilibrium in the REV, can be written as;

$$\left(\rho\, C_P\right)_m \nabla.(VT) = \nabla.(k_\varepsilon \nabla T) \text{....(7)}$$

where (k_ε) is the effective thermal conductivity, and T is the temperature in the REV, and the volumetric heat capacity (C_p) is considered for the fluid and the solid. The effective conductivity k_ε of saturated metal foams is calculated from conductive heat transfer through the medium (i.e. for the fluid in static conditions) Nithiarasu et al. [17];

$$\left(\rho\, C_p\right)_m = \varepsilon\left(\rho\, C_p\right)_f + (1-\varepsilon)\left(\rho\, C_p\right)_s \text{.....(8)}$$

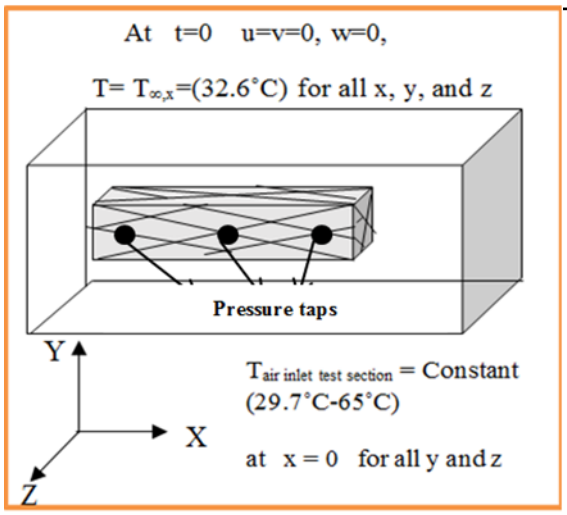

Figure (2): Model with Meshes

Boundary Conditions

In the commercial package Comsol Multiphysics 4.3b, the boundary conditions of the present problem used are;

1. The default interior medium is the copper foams with given values of the permeability and the thickness of copper foams zone.
2. The air has been chosen as the fluid inside copper foams with its properties known at all temperatures used.
3. Four heaters (220 volts , 1800 watt for each heater) are placed in duct before test section where the temperature was assigned for the heaters and changed at each case to get a constant temperature at inlet for air and dusty air, and the duct covered by glass wool in order not to burns; (Length : 120cm, diameter: 5mm, inconeal 800, tetanium stainless steel)
4. Inlet boundary: Inlet absolute pressure is specified as the inlet boundary condition, total temperature (room temperature). Outlet boundary: The outflow velocity is specified and laminar flow values of pore Reynolds number of clean air for (10PPI) are (119.10, 168, 218, 306.8, and 356.7) and for (40PPI) are (73.8, 104.2, 135.21, 190.3, and 221.3) and for dusty air (10PPI)(416.17).
5. Box wood walls (duct contains copper foams): stationary wall, no slip and insulated.

EXPERIMENTAL WORK:

Experimental work had been performed to investigate the problem and explore the effect of various parameters. The experimental apparatus includes the wind tunnel shown photographically in plate (1), dusty air system, see plate (2), the model, the working section and the instrumentation. An experimental rig was constructed in the Heat Transfer Lab, at the Mechanical Engineering Department, University of Baghdad were the experiments carried out. A centrifugal blower (AUGUSTO CATTANI) of (2.5 cm) diameter was used to supply the air to the dusty air system (dust storage tank and dust control valve). The dust concentrations were with different dust ratio values (density number N) of (2, 4, 6 and 8). The test section was made from Pyrex material with

dimensions (300 mm × 150 mm) and 294 mm length.

The mean velocity at the test section used in the present work was (2.23, 3.16, 4.08, 5.77 and 6.7 m/s) at the valve openings (20%, 40%, 60%, 80% and 100%) respectively. A digital manometer (Dwyer) (with uncertainty ± 0.001 m/s) was used to measure the wind tunnel mean air velocity in duct. The pore Reynolds number based on these velocities for (10PPI) are (119.1, 168, 218, 306.8, and 356.7), and for (40PPI) are (73.8, 104.21, 135.21, 190.3, and 221.3), see table (1). Four heaters were used to get constant inlet air temperature with values (29.7˚C, 40˚C, 50˚C, 60˚C, 65˚C). Measurements were made for the copper foams samples of (10PPI & 40PPI) to measure porosity (ε)and density, and by using (ASTM D3574-03), examination of the purity of the copper foams was made by using the x-ray diffraction apparatus (LabX-XRD-6100X-ray diffractometer), examination of the number of pores per inch (PPI) was made by using the scanning electron microscope (SEM) apparatus, the dust density (N) measured by filter fixed at dusty air system by made by Salman [15], and the effective thermal conductivity (k) used by Wajeeh [18] was used ;

$$k_{eff} = \varepsilon k_f + (1-\varepsilon)k_s \quad .....(8)$$

Where;

k_{eff} = Effective thermal conductivity of air and copper foams.

k_s= Thermal conductivity of the copper foams (401 W/m.k).

k_f = Thermal conductivity of Air (0.02605 W/m.k).

The temperature distribution of the enclosure test section were measured by twelve thermocouples wire (type K), one of the thermocouple used to measure the temperature at inlet clean air or dusty air and these are conncted to a one temperature data reader, contains 12 channels temperature recorder of the model BTM-4208SD with uncertainty ±0.335˚C. The measured temperatures are recorded by this real time temperature recorder on SD Memory Card and also recorded and displayed, see figure (3). Table (2) represents thermal properties of dusty air as a mixture with discharge of air (7.02m^3/hr), see equation (6). The percentage of dust or the clean air (%) calculated by mixture laws. Three U-Tube Manometers (with uncertainty ± 0.1 mmH_2O) where used to measure the gauge pressure along the flow direction (x-axis) with a uniform spacing of (60 mm), see figure (2) and then calculated absolute pressure as below;

$$(P_{absolute} - P_{atm} = \gamma_w \Delta h) = P_{gauge} .....(9)$$

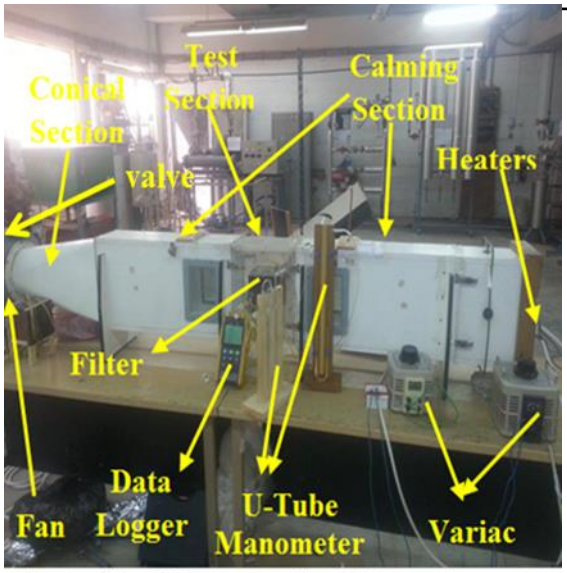

Plate (1): Photograph of Experimental Apparatus

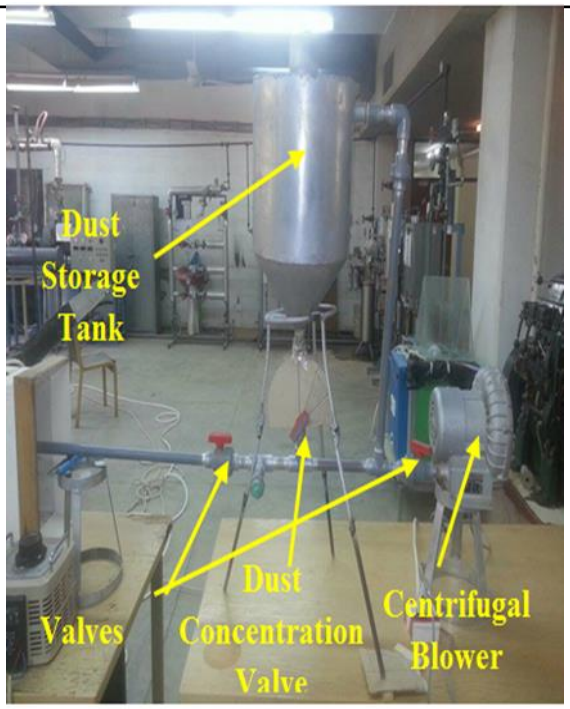

Plate (2): Dusty Air System

Table (1): Properties of Copper Foams

Parameters	10ppi	40ppi
Porosity (ε)	0.90	0.89
Permeability (K)	4.27×10^{-7} (m^2)	1.28×10^{-7} (m^2)
Friction Coefficient (C_f)	0.1665178	0.16989
Forchheimer Form Drag Coefficient (C)	254.55 (m^{-1})	474.19 (m^{-1})
Density (ρ)	8663 (kg/m^3	9095 (kg/m
Thermal Conductivity (k	401(W /m.C)	401(W /m.C)
Specific Heat Capacity (C_p)	385 (J/kg.C	385 (J/kg.C
Average pore Diameter (D_p)	905.7 µm	568.6 µm

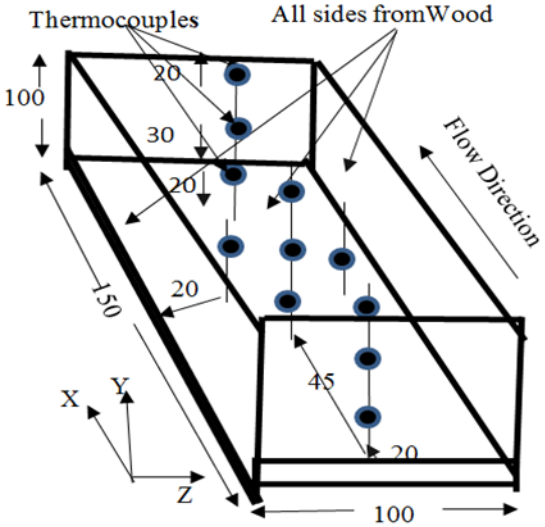

Figure (3): Thermocouples Location (dimensions in mm)

Table (2): Thermal Properties of Dusty Air

%Air	98.447	96.941	95.481	94.064
%Dust	1.552	3.058	4.518	5.935
C (g/m^3)	17.09	34.188	51.28	68.376
N (g/min)	2	4	6	8
C_p (kJ/kg.°c)	1.021	1.034	1.047	1.060
k (W/m.°c)	0.0287	0.0292	0.0297	0.0302
ρ (kg/m^3)	1.067	1.0514	1.0369	1.0233

Results and Discussion:

Numerical Results:

Figures (4) and (5) for copper foam clean air filter (10PPI) at 29.7˚C and 65˚C respectively represent the surface contours map of absolute pressure for different Reynolds Number, the figures show that the air pressure are higher and gradually decreased with air flow, the increment caused by chocking the air flow to the solid matrix of copper foam filter at high velocity. The pressure drop inside the copper foam filter increased by increasing the Reynolds Number. The figures (6) and (7) for copper foam clean air filter (40PPI) at 29.7˚C and 65˚C respectively show the surface contour map of pressure for different Openings ratio, where the pressure drop inside the copper foam filter increased with increasing the Reynolds Number. The figure (8) represents the surface contour map pressure for copper foam dusty air filter of 10PPI for velocity 8m/s and inlet air temperature (53˚C), the absolute pressure increased with increasing the concentration of dust particles in air with constant dusty air velocity. The figure (9) represents the surface contour map pressure for copper foam dust air filter of 40PPI for velocity 8m/s and inlet air temperature (53˚C), the absolute pressure increased with increasing the concentration of particles dust in air with constant dusty air velocity. The figures (10) and (11) represent the comparison of pressure distribution between the copper foam with clean air (10PPI & 40PPI) at 29.7˚C and 65˚C respectively. It is clear that the pressure drop for the 40PPI is higher than the 10PPI and increases with increasing the Reynolds Number because of the decrease in the permeability (increase the pore density & increase the pore diameter of foam) causing the higher pressure drop in 40PPI, where this results verify the last term of Forchhiemer equation (4)

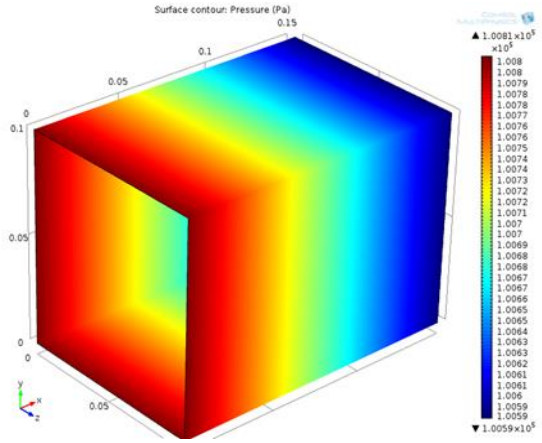

(a): Openings 20%

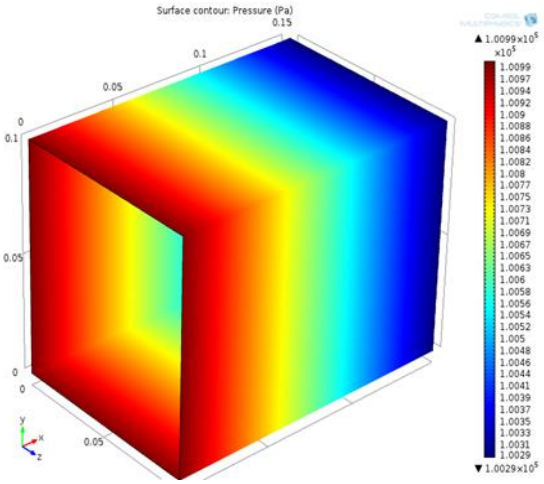

(c): Openings 60%

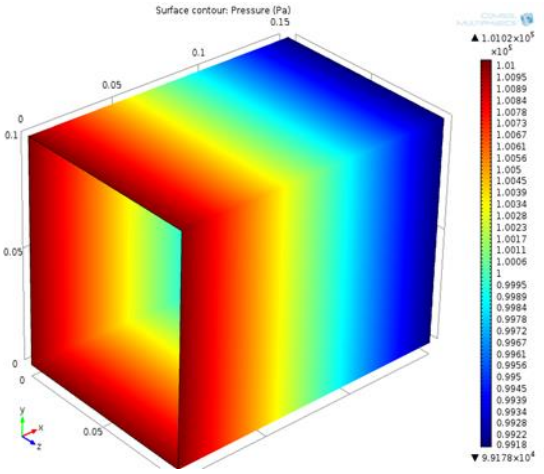

(e): Openings 100%

Figure (4): Surface Contour Pressure for 10PPI and Different Openings Ratio at (29.7˚C) (Clean Air)

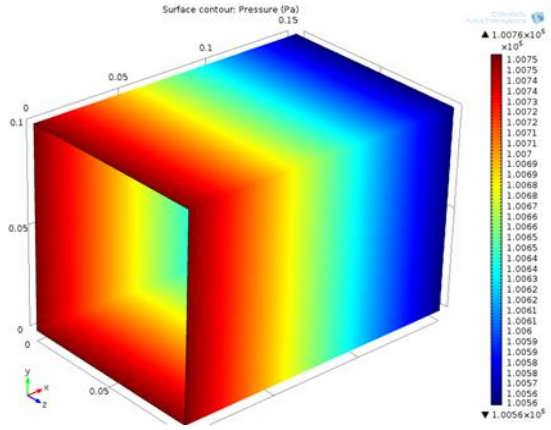

(a): Openings 20%

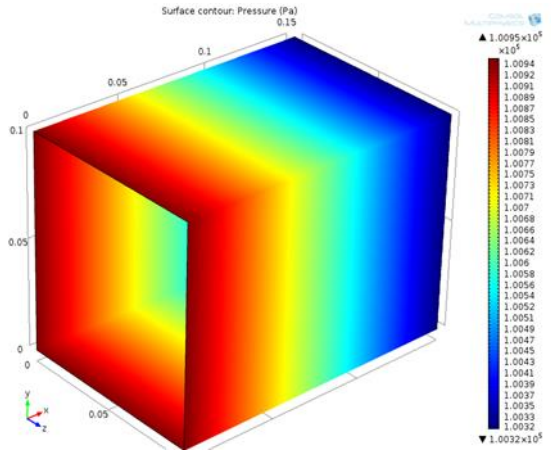

(c): Openings 60%

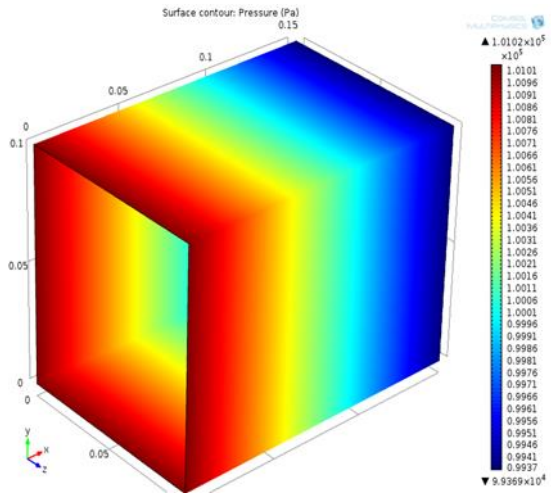

(e): Openings 100%

Figure (5): Surface Contour Pressure for 10PPI and Different Openings Ratio at (65˚C) (Clean Air)

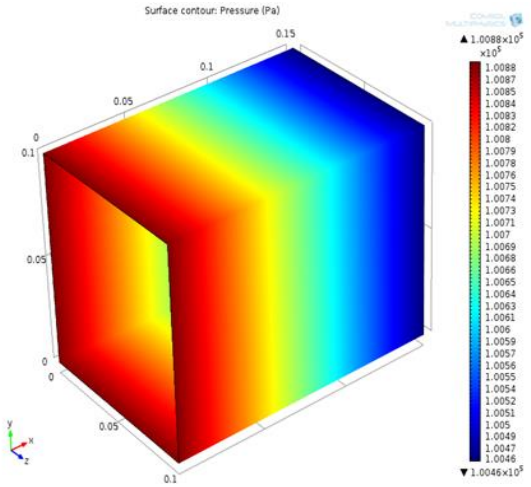

(a): Openings 20%

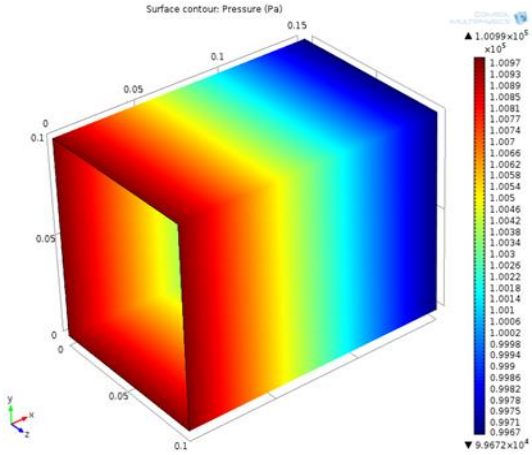

(c): Openings 60%

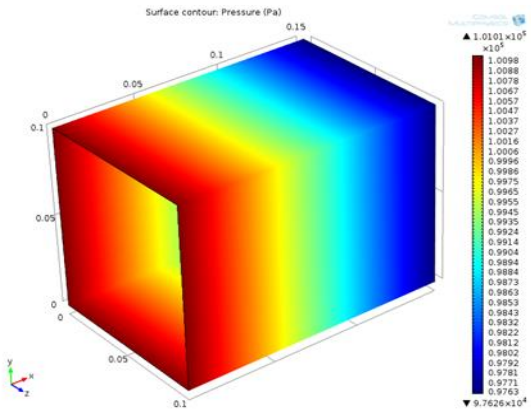

(e): Openings 100%

Figure (6): Surface Contour Pressure for 40PPI Different Openings Ratio at (29.7˚C) (Clean Air)

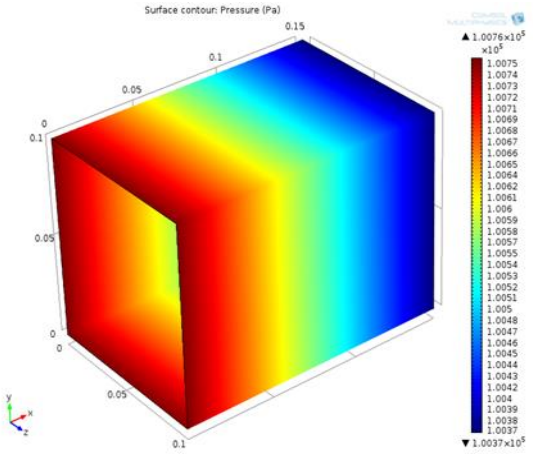

(a): Openings 20%

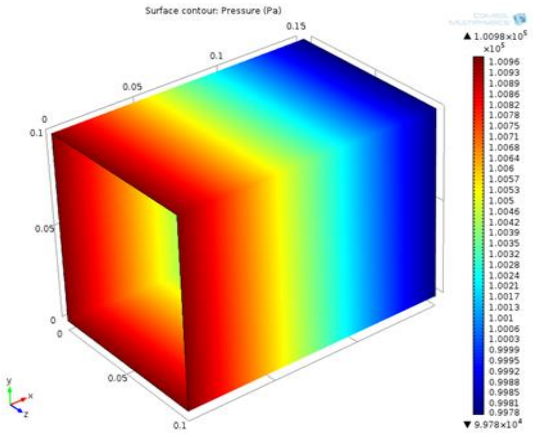

(c): Openings 60%

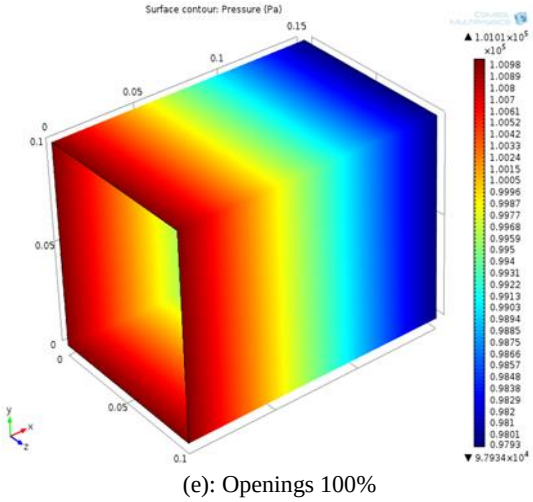

(e): Openings 100%

Figure (7): Surface Contour Pressure for 40PPI Different Openings Ratio at (65˚C) (Clean Air)

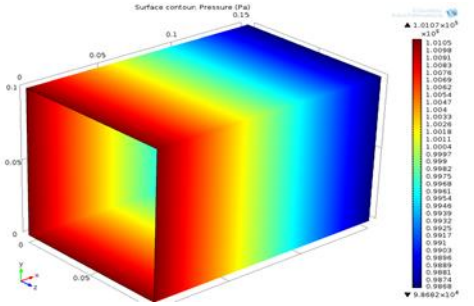

(a): with N= 2

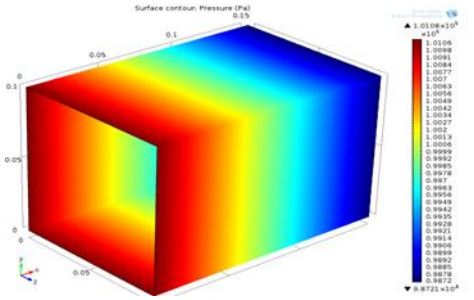

(b): with N= 4

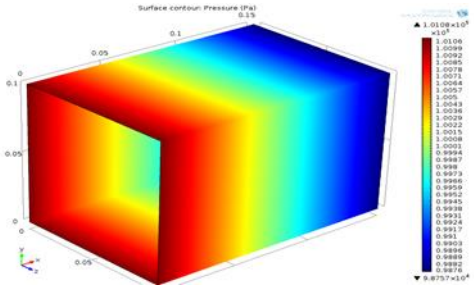

(c): with N= 6

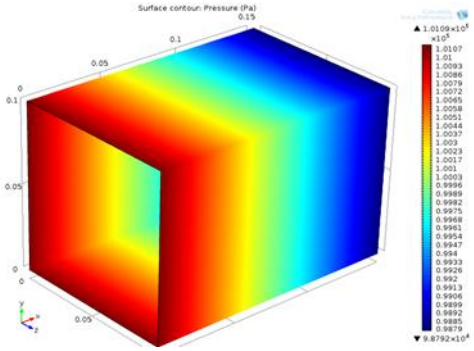

(d): with N= 8

Figure (8): Surface Contour Pressure for Dusty Air Flow through Copper Foam Filter of 10PPI for Different Dust Concentrations and Temperature 53˚C & Velocity 8m/s

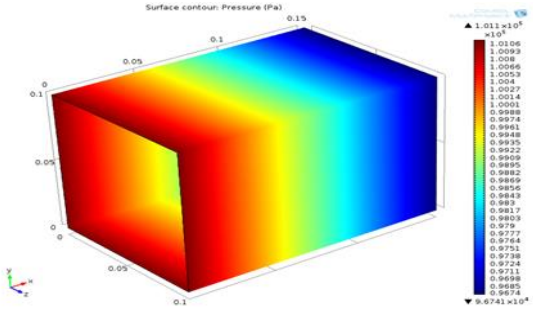

(a): with N=2

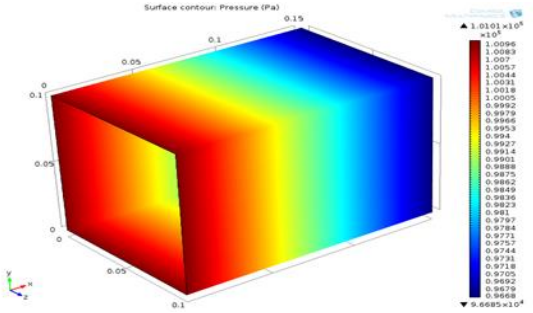

(b): with N=4

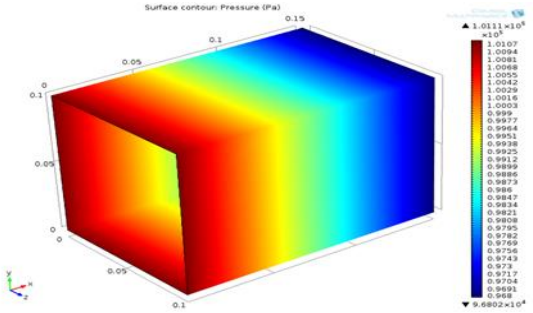

(c): with N=6

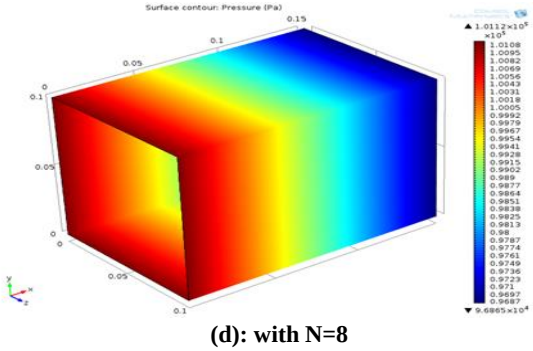

(d): with N=8

Figure (9): Surface Contour Pressure for Dusty Air Flow through Copper Foam Filter of 40PPI for Different Dust Concentrations and Temperature 53˚C & Velocity 8m/s

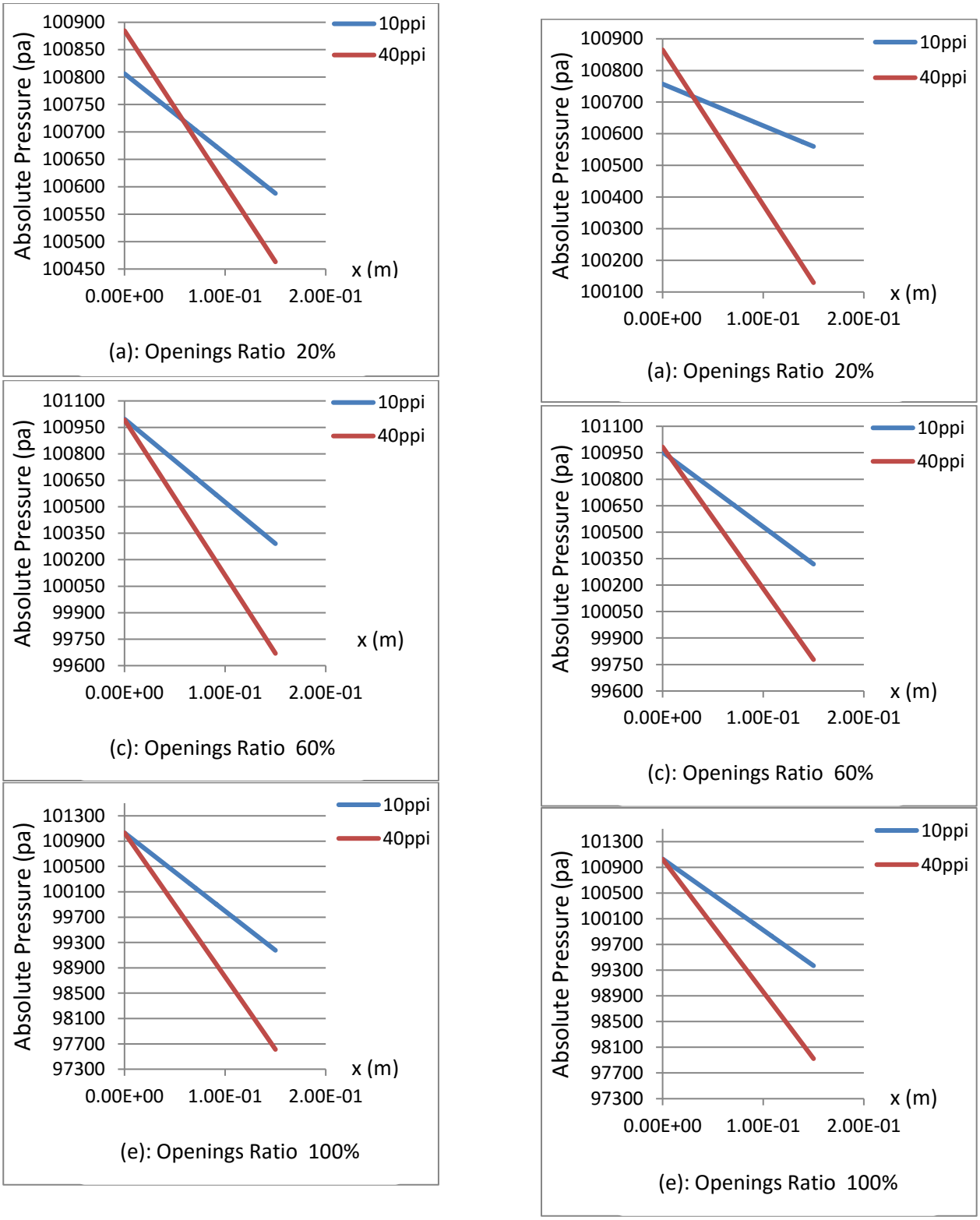

Figure (10): Effect of PPI of Numerical Results at Different Openings Ratio for 29.7˚C

Figure (11): Effect of PPI of Numerical Results at Different Openings Ratio for 65˚C

Experimental Results

In the experimental part of the present work, a total of 58 test runs were carried out to cover all the possible investigated parameters. For the pressure drop distribution, figure (12) represents the copper foams filter (10PPI) of clean air with constant inlet air temperature for five values of the openings. It is clear that the full openings (100%) for all temperatures gives the higher absolute pressures except at (60˚C), and generally, the absolute pressure increases with increasing the openings and increasing the inlet air temperatures, the increase in absolute pressure is because of the increasing in Reynolds Number and as a result of the presence of the solid matrix in the path of the air flow. The flow absolute pressure depends on the size and shape of pores and cells, length and cross section of ligaments and all of these are connected to form a network of cells inside metal foams. Figure (13) represents the results of copper foams filter (40PPI) of clean air with constant inlet air temperature for different values of openings. The absolute pressure with x-axis in all cases are higher at the full openings (100%), and 65˚C represents the higher absolute pressure and the differences between the curves became clear. Generally the absolute pressure curves are decreasing by small values in the flow direction with increased inlet air temperature and increased values of the openings, this behavior of foams filter is because of the low permeability and chocked of the air flow by solid matrix of the foams (ligaments) and the change of the cross section of the ligament caused this rise in the absolute pressure. The figures (14) and (15) show the results for the copper foam filter (10PPI & 40PPI) of dusty air with different dust concentrations and constant inlet air temperature 53˚C and velocity 8m/s, the figures show that the increase in the dust concentration causes an increase in the absolute pressure, where the higher pressure obtained at higher dust concentration especially in 40PPI because the particles of dust blocks the pores in copper foam filter gradually causing high absolute pressure. For the temperature distribution, figures (16) to (19), the temperatures of the (10PPI & 40PPI) with openings (20% & 100%) and constant inlet air temperature ($T\infty$=40˚C, $T\infty$=65˚C) in clean air are approximately constant or close in all cases because there is no source or sink of heat in the flow, the temperature curves are increased at 100% with 65˚C & 40˚C, this increase caused by non-uniform size and shape of pores and ligaments and these caused good mixing for the flow. For dusty air with constant inlet air temperature 53˚C and two dust concentrations (N=4 & N=8), see figures (20) and (21), the temperature distributions in copper foam filter are close in all the cases

with two dust concentrations, but the temperature in the metal foam filter decreased in 40PPI more than the 10PPI because of the presence of the dust particles in air caused reduction in the temperature. It is noted that as the pore density increases (increases the surface to volume ratio, which increases the flow resistance by lowering the permeability). For the effect of PPI on the experimental results, figures (22) to (25) represent a comparison between copper foam filter behavior for clean air of (10PPI & 40PPI), the values of the absolute pressures for (40PPI) are higher than that for the (10PPI) with increasing values of the Reynolds Number because of the low resistance to airflow in 10PPI compared to high resistance for 40PPI. It is noted that as the pore density increases (increases the surface to volume ratio, which increases the flow resistance by lowering the permeability), the pressure drop increases with increasing air velocity. This is given by an increase in the tortuosity or obstruction of air flow through the sample. Further, in the filter with dusty air, see figure (26), the absolute pressure of the (10PPI &40PPI) increased with increasing (N) and the absolute pressure in copper foam dusty air filter of 40PPI is higher than that for 10PPI because of the presence of particles of dust in air caused to high absolute pressure especially in 40PPI. For the effect of dust on the experimental results, The figures (27) and (28) represent the pressure distribution of dusty air with (low concentration N=2&high concentration N=8) at 53˚C & 8m/s, and with clean air at 50˚C & 6.71m/s for 10PPI and 40PPI respectively. It is clear from the curves of dusty air with N=8 that the absolute pressure is higher at all points, and the curves of dusty air at N=2 & N=8 at 40PPI are steeper than that for 10PPI, this is because of the presence of dust particles with air that enters the copper foam filter, and choking, accumulating the dusty air in 40PPI because of the presence of the high number of pores.

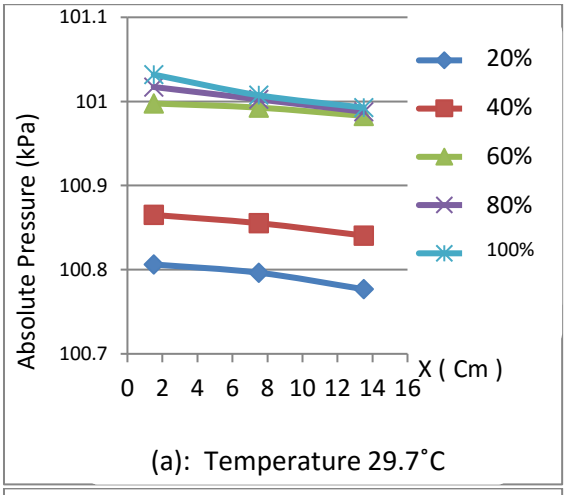

(a): Temperature 29.7˚C

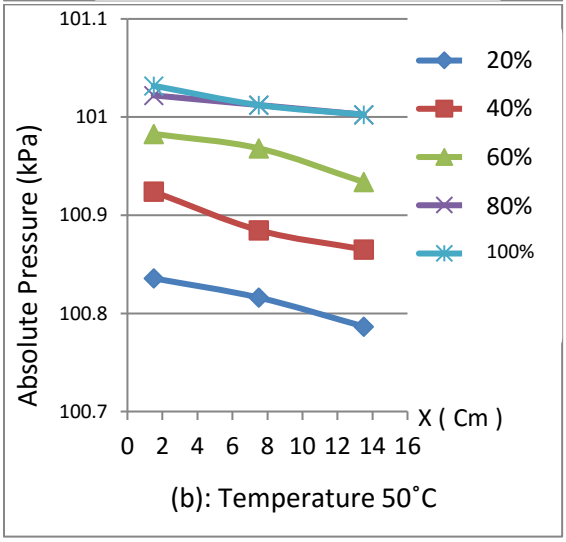

(b): Temperature 50˚C

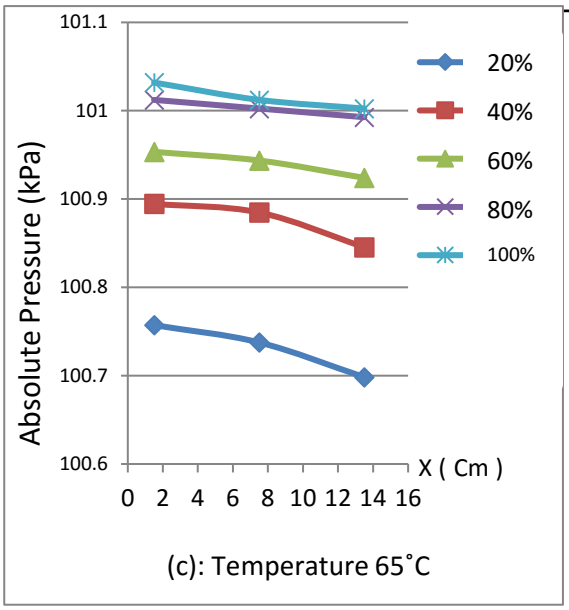

Figure (12): Pressure Distribution at Constant Inlet Clean Air Temperature with Different Openings Ratio for (10PPI)

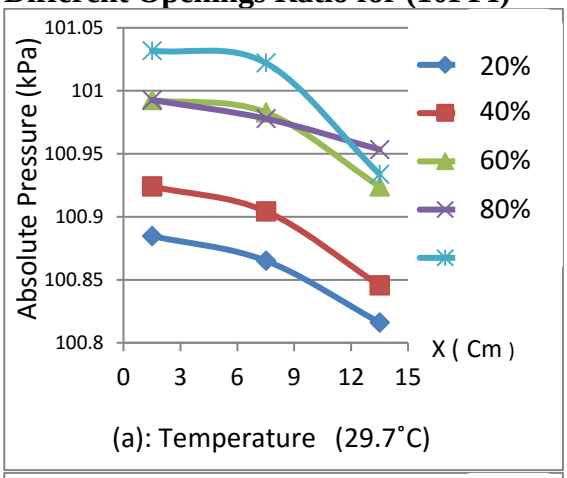

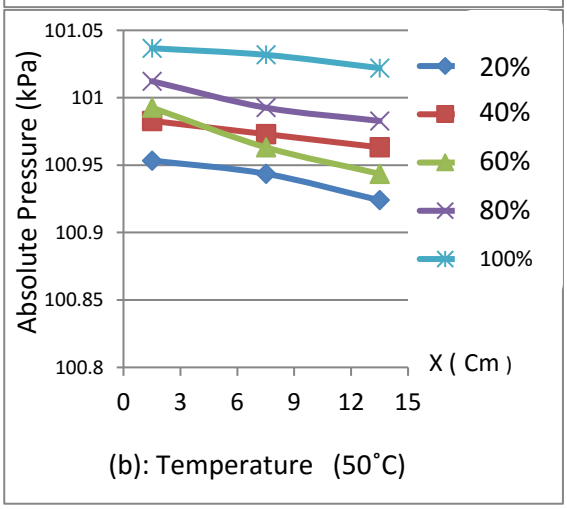

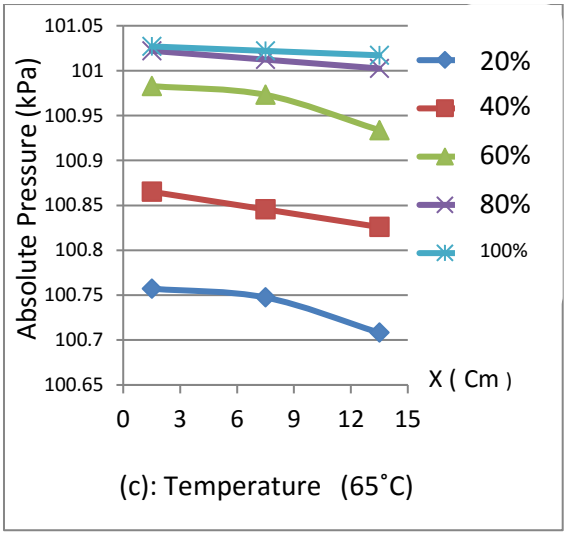

Figure (13): Pressure Distribution at Constant Inlet Clean Air Temperature with Different Openings Ratio for (40PPI)

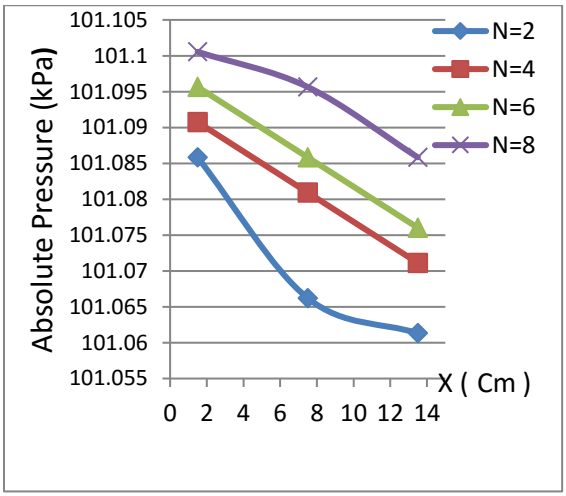

Figure (14): Pressure Distribution of Dusty Air at Constant Inlet Air Temperature (53˚C) with Different Dust Concentrations and with Velocity (8 m/s) for (10PPI)

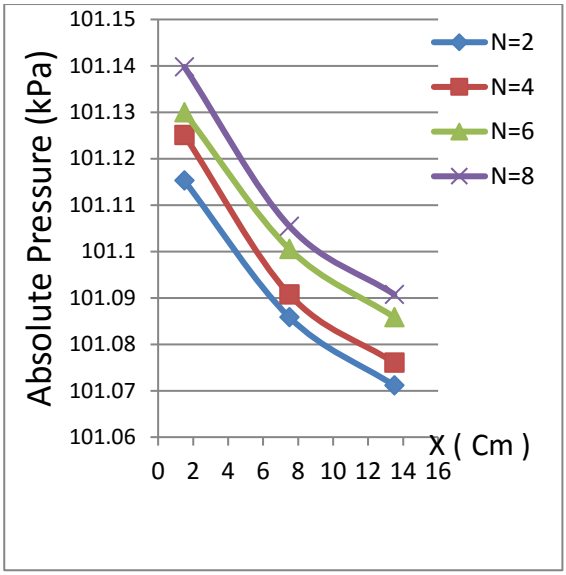

Figure (15): Pressure Distribution of Dusty Air at Constant Inlet Air Temperature (53˚C) with Different Dust Concentrations and Velocity (8 m/s) for (40PPI)

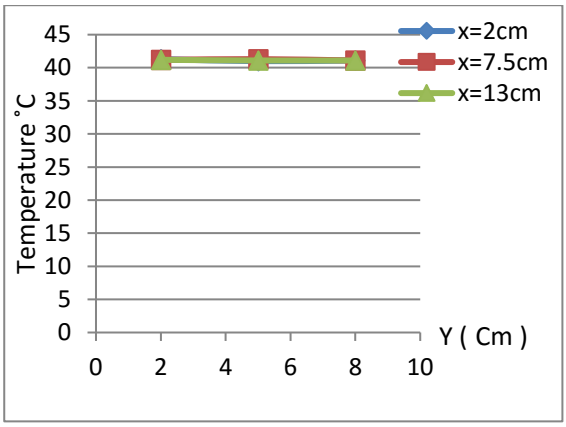

Figure (16): Temperature Distributions of Clean Air for (10PPI) and Openings Ratio 20%& 40˚C

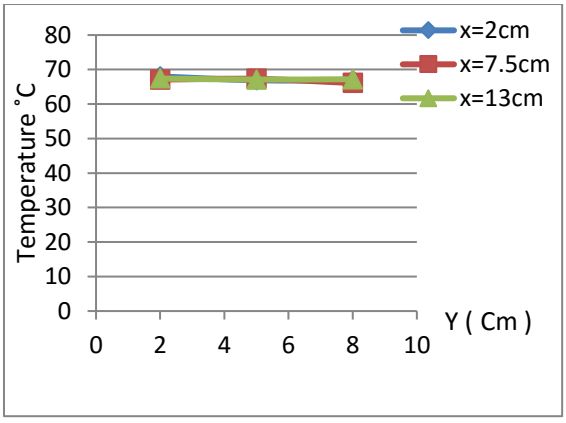

Figure(17): Temperature Distributions of Clean Air for (10PPI) and Openings Ratio 100%& 65˚C

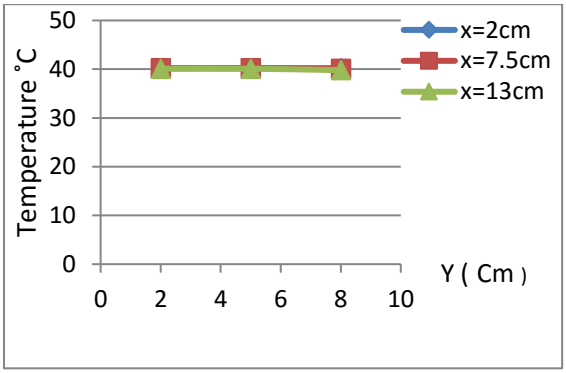

Figure(18): Temperature Distributions of Clean Air for (40PPI) and Openings Ratio 20% & 40˚C

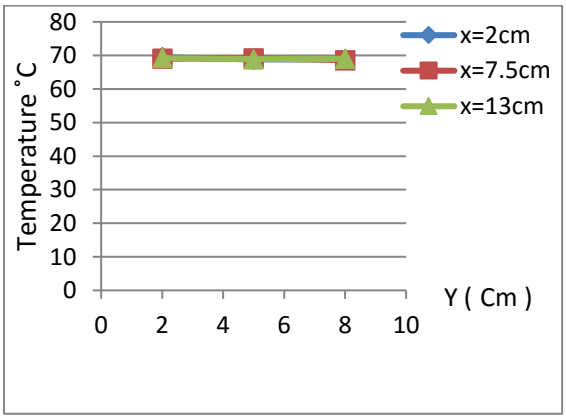

Figure(19): Temperature Distributions of Clean Air for (40PPI) and Openings 100%& 65˚C

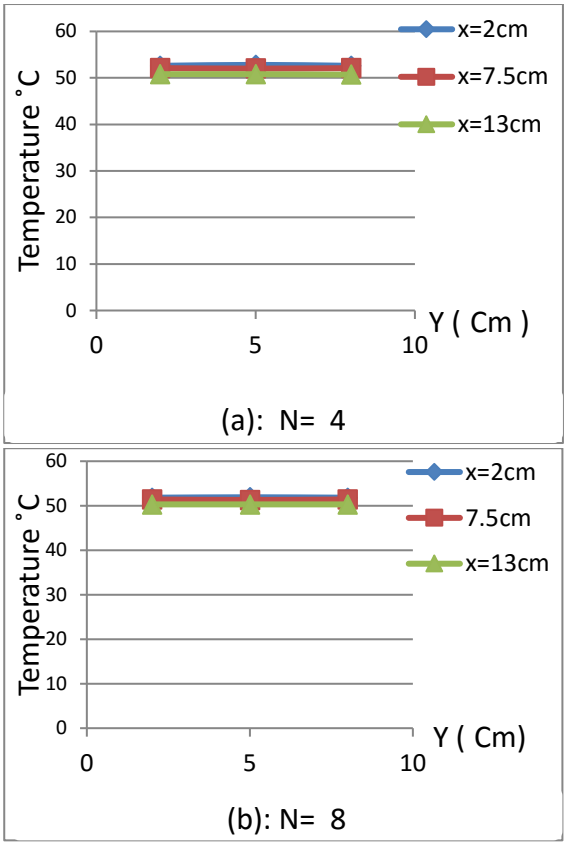

Figure (20): Temperature Distribution of Dusty Air at Constant Inlet Air Temperature (53˚C) with Different Dust Concentrations for (10PPI)

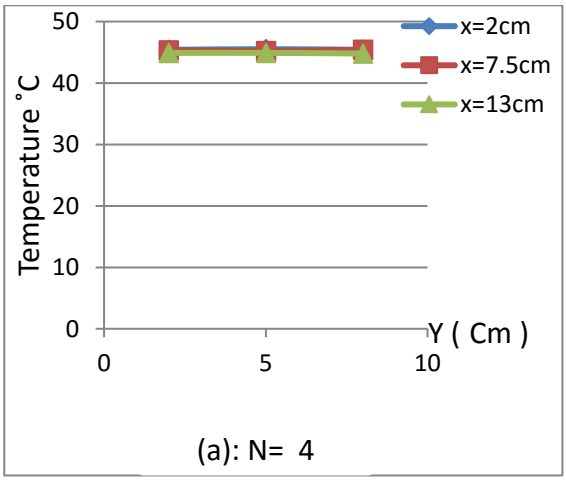

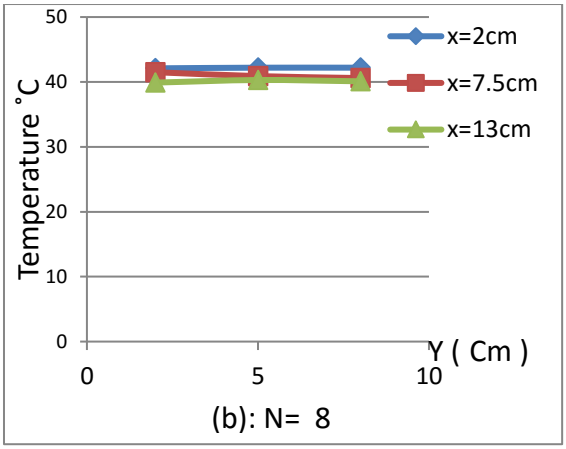

Figure (21): Temperature Distribution of Dusty Air at Constant Inlet Air Temperature (53˚C) with Different Dust Concentrations for (40PPI)

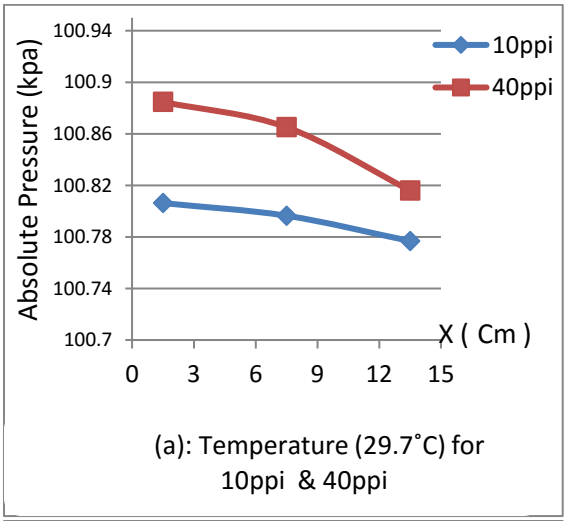

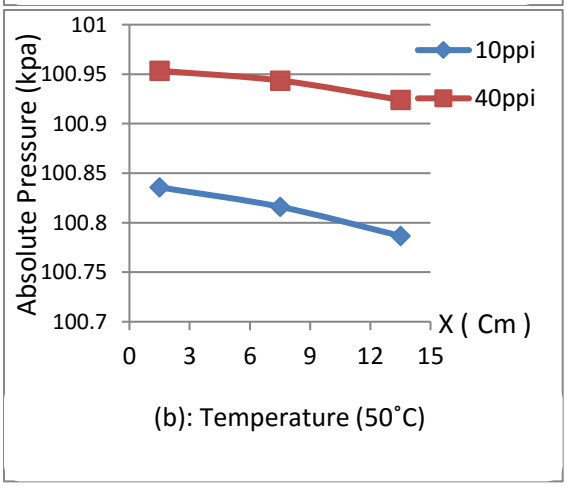

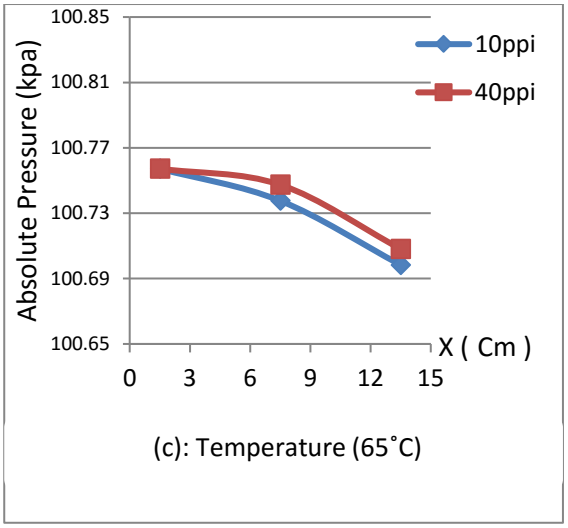

Figure (22): Effect of PPI of Experimental Results at Opening Ratio (20%) with Different Temperatures (Clean Air).

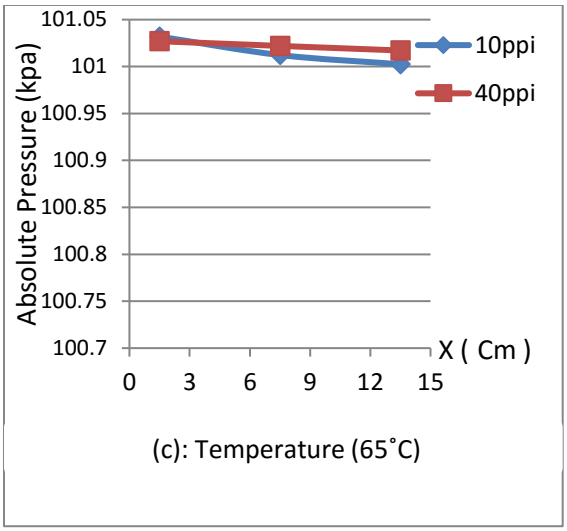

Figure (23): Effect of PPI of Experimental Results at Opening Ratio (100%) with Different Temperatures (Clean Air).

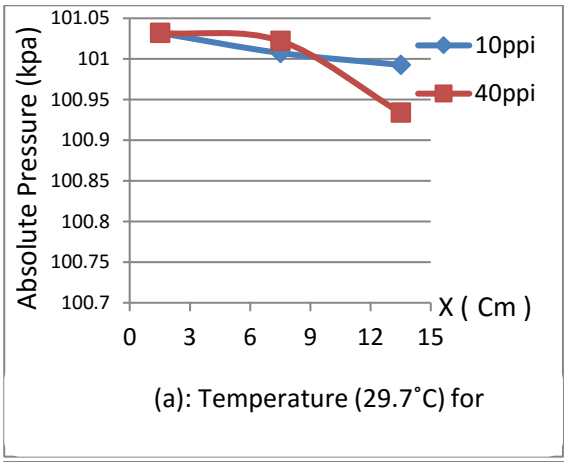

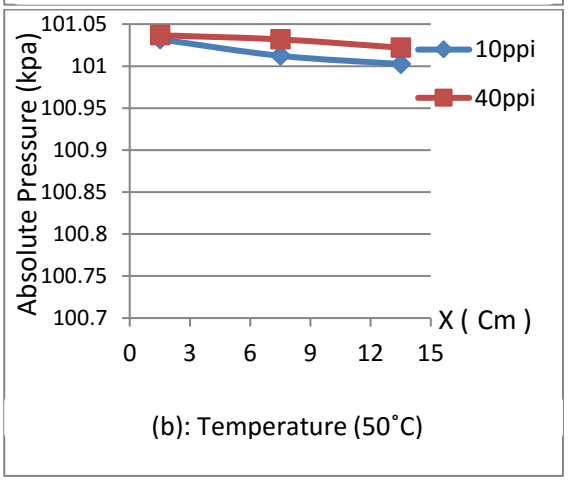

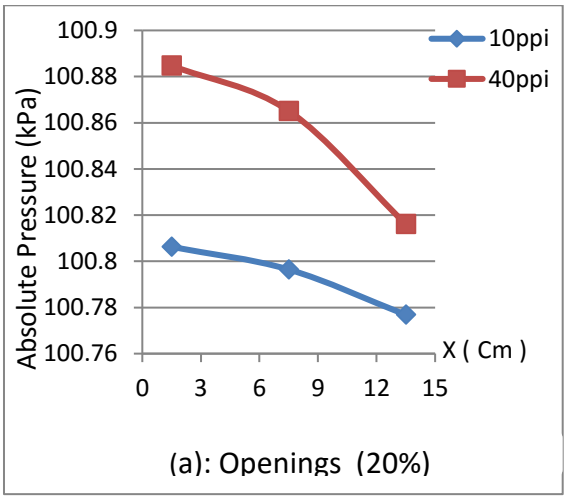

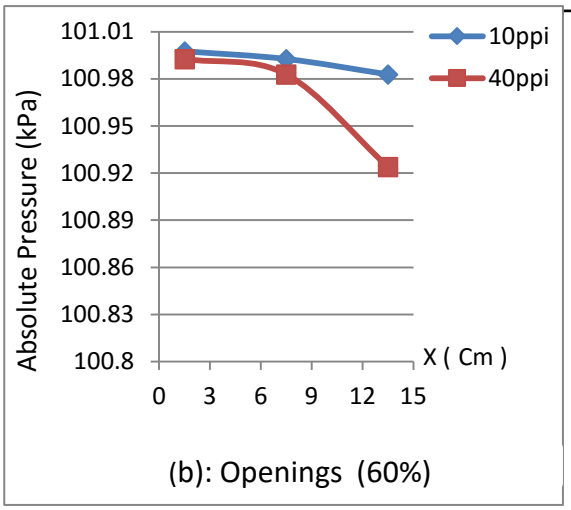

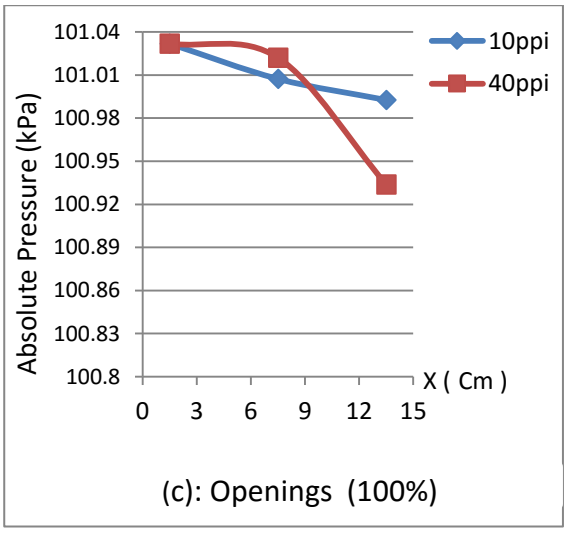

Figure (24): Effect of PPI of Experimental Results at Inlet Clean Air Temperature (29.7˚C) with Different Openings Ratio

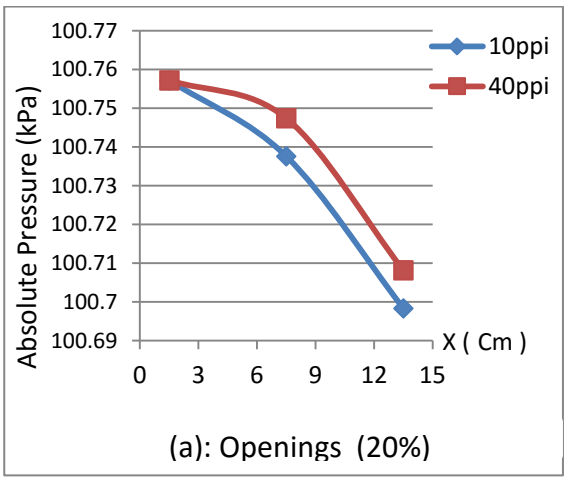

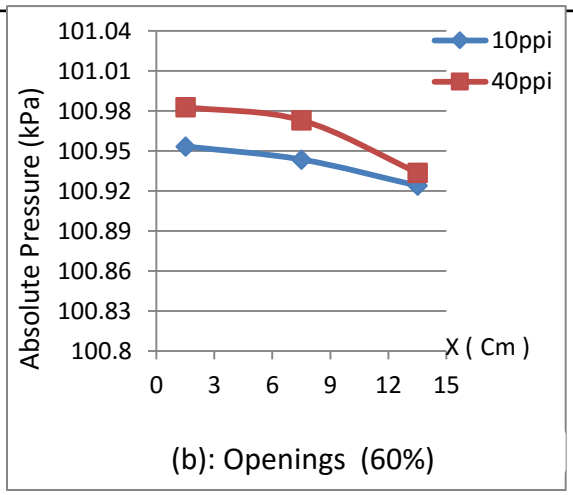

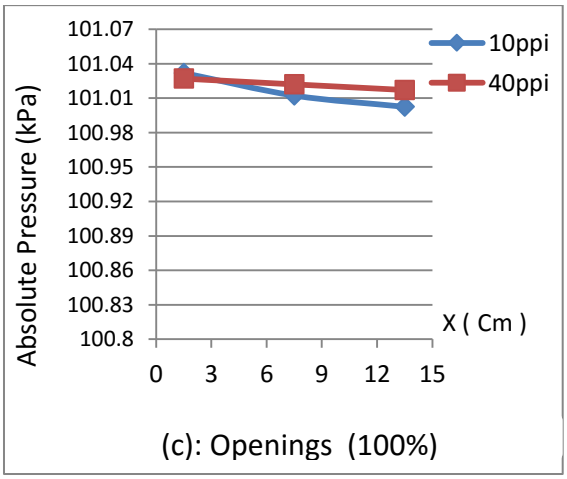

Figure (25): Effect of PPI of Experimental Results at Inlet Clean Air Temperature (65˚C) with Different Openings Ratio

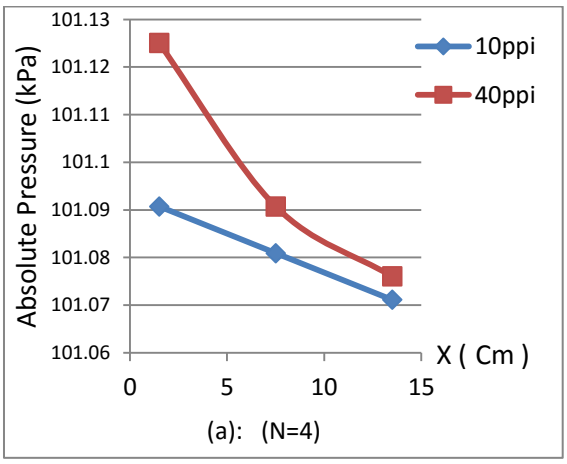

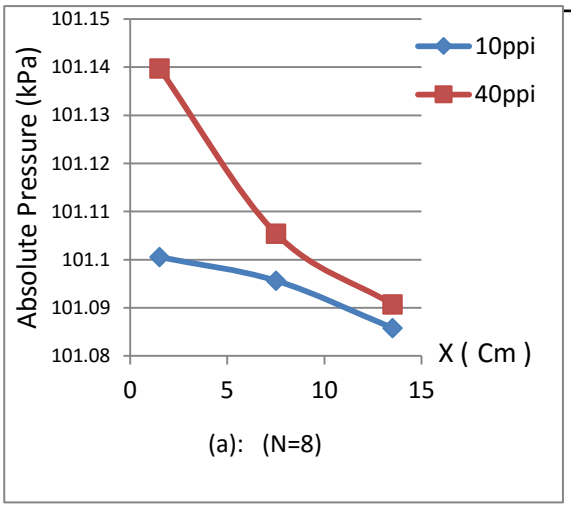

Figure (26): Effect of PPI of Experimental Results of Dusty Air at Different Dust Concentrations and (N) for Velocity (8 m/s)

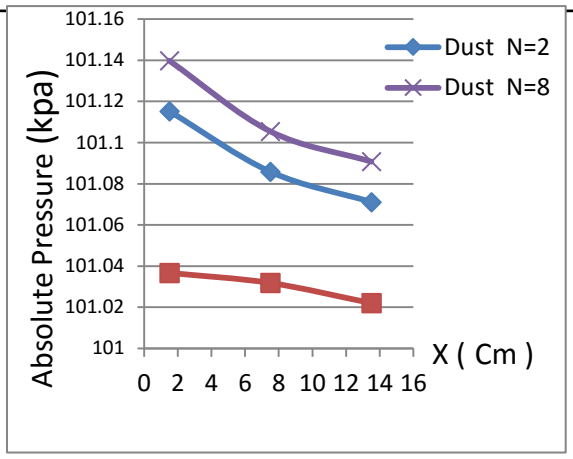

Figure (28): Pressure Distribution of Dusty Air with Different Dust Concentrations at (53˚C & 8 m/s) and Clean Air at (50˚C & 6.71 m/s) for (40PPI)

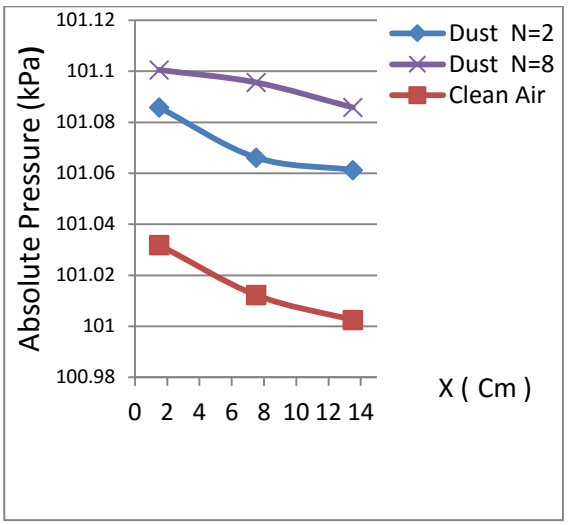

Figure (27): Pressure Distribution of Dusty Air with Different Dust Concentrations at (53˚C & 8 m/s) and Clean Air at (50˚C & 6.71 m/s) for (10PPI)

Verification:

Figures (29) and (30) represent a comparison of the pressure distribution between the experimental and numerical results for 10PPI and 40PPI at Openings ratio (20% & 100%) and different inlet air temperature (29.7˚C & 65˚C) for clean and dusty air, where the experimental data has been used to run the program and obtain numerical results for test case of the experiment. Figures reveal that the numerical surface contours map of pressure follows the same behavior as the present experimental results but is approximately with a mean of difference 1-5%.

To verify the results obtained from the present study, a comparison was made with the results achieved by previous studies. The present results for the pressure distribution for clean air shown in figures (31) and (32) experimentally and numerically agrees

with results of **Andrea et al. [4]** for numerical study shown in figure. (33).

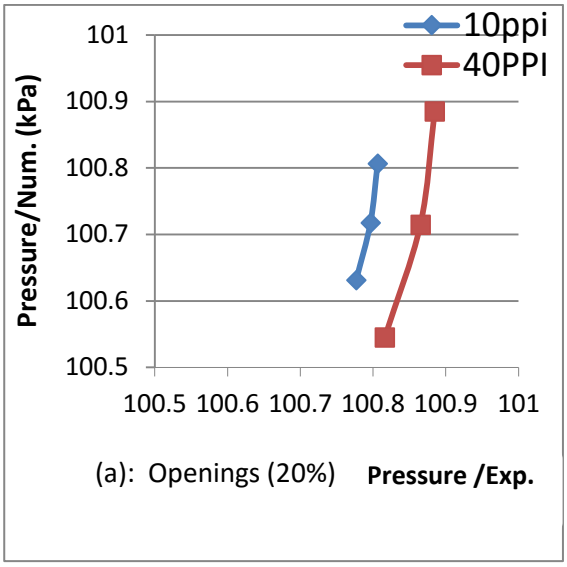

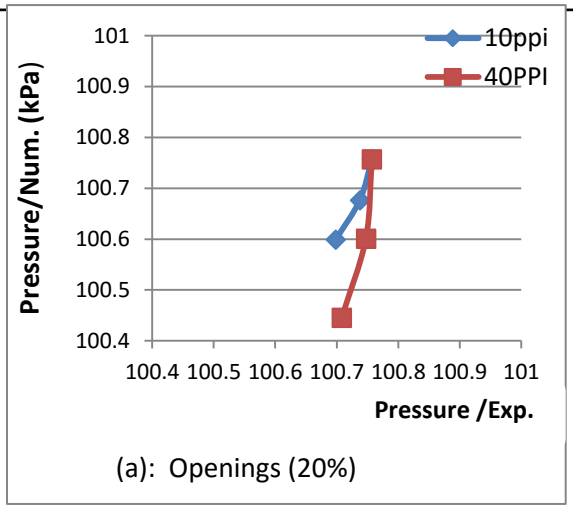

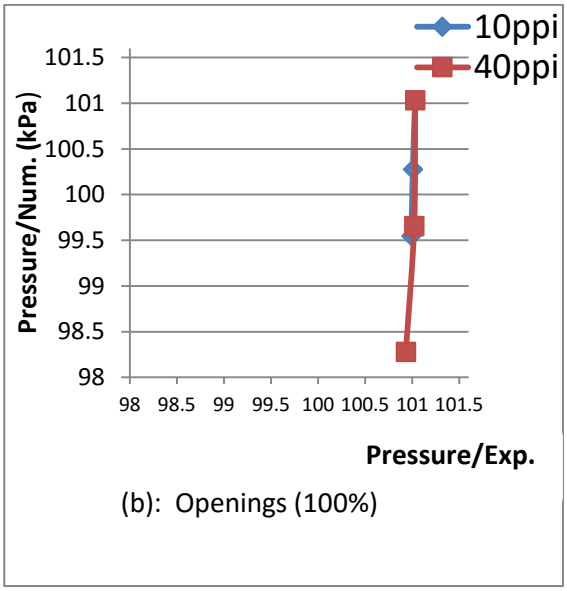

Figure (29): Comparison between 10PPI and 40PPI (Experimental & Numerical) for 29.7˚C (Clean Air)

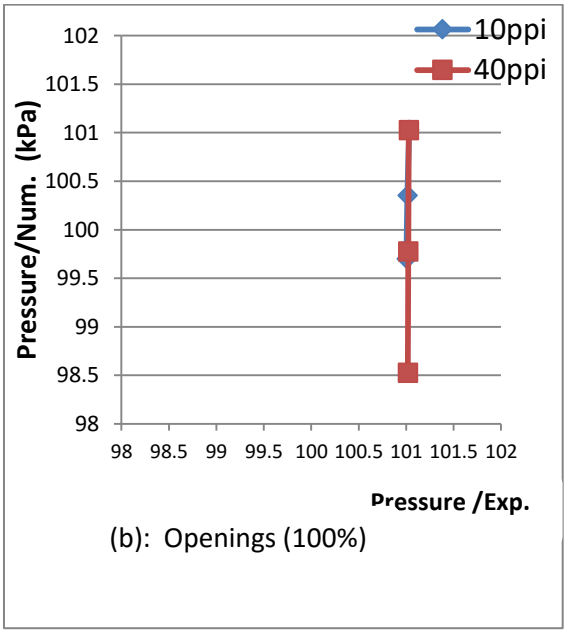

Figure (30): Comparison between 10PPI and 40PPI (Experimental & Numerical) for 65˚C (Clean Air)

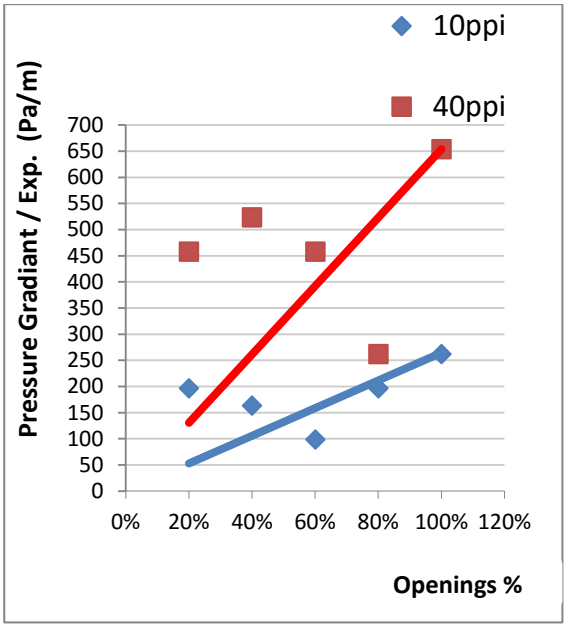

Figure (31): Pressure Gradiant Experimental Comparison between 10PPI and 40PPI at Temperature (29.7˚C) for Clean Air.

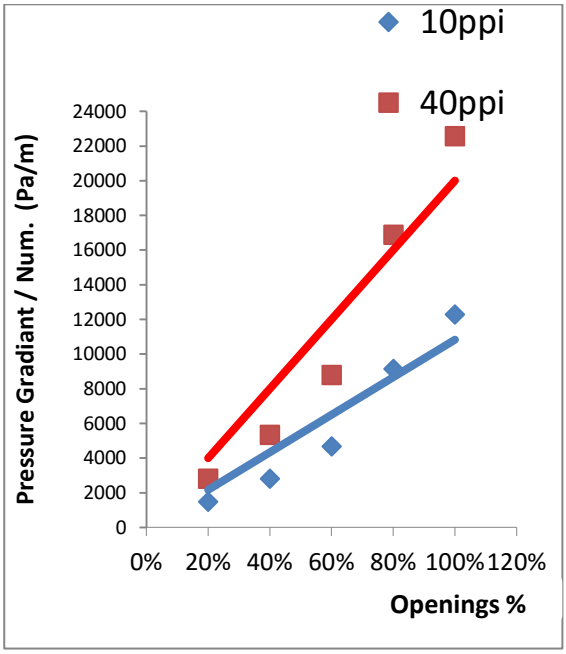

Figure (32): Pressure Gradiant Numerical Comparison between 10PPI and 40PPI at Temperature (29.7˚C) for Clean Air.

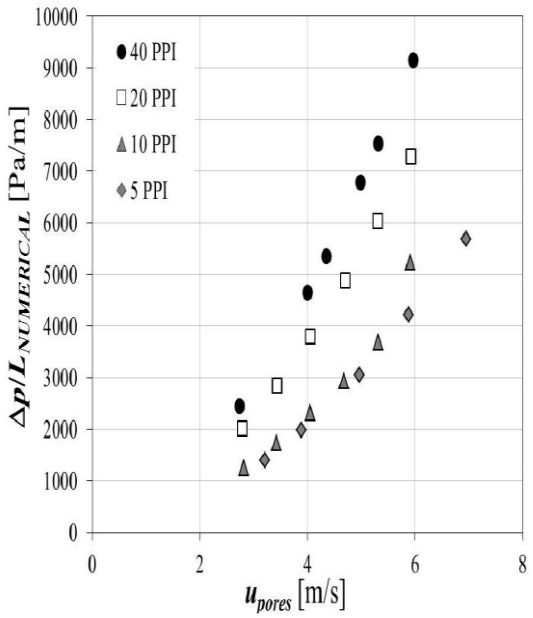

Figure (33): Numerical Pressure Gradiant with pore velocity of Metal Foams for Different Pore Densities (Andrea et al. 2014)

Conclusions:

1. The temperature of convective air flow and copper foams in the axial direction decreases (slightly) at all temperatures in clean and dusty air for (10PPI & 40PPI).
2. The pressure of the copper foam filter with 40PPI is higher than the copper foam filter with 10PPI at all values of Reynolds Number and all temperatures, the pressure increases with increasing dust concentration (C) or dust density (N= 2, 4, 6 & 8).
3. The pressure through copper foam filter with 40PPI is higher than the

10PPI, and the pressure for dusty air at dust density (N= 2 & 4) is higher than the clean air at same conditions.

4. The pressure drop for the copper foam filter with 40PPI is higher than the copper foam filter with 10PPI.
5. In the present work, the numerical pressure drop in copper foam filter is higher than that obtained experimentally for clean and dusty air.
6. The permeability increases almost linearly with increasing the pore diameter at fixed porosity. Comparison gave a good agreement between the present and previous works.

Nomenclature:

c_p Specific Heat Capacity
C Dust particle concentration
d_p Average Diameter of pores for copper foam filter (Hydraulic Diameter) or characteristic Length
K Permeability
K_{eff} Effective thermal conductivity of copper foams
N Density Number (Dust Ratio)
P Pressure
PPI Pore per inch for Copper Foams
x, y, z Cartesian coordinate system
ε Porosity
C_F The Forchheimer's Coefficient (form drag)

References:

[1] A. Kopanidis, A. Theodorakakos, E. Gavaises, D. Bouris, "3D Numerical Simulation of Flow and Conjugate Heat Transfer Through a Pore Scale Model of High Porosity Open Cell Metal Foam." Elsevier, International Journal of Heat and Mass Transfer 53 (2010) 2539–2550.

[2] Lee, J.M., Sung, N.W., Cho, G.B., &Oh, K.O., "Performance of Radial-Type Metal Foam Diesel Particulate Filters.", International Journal of Automotive Technology-Korea, 11, 307–316, 2010.

[3] Anurag Dubey and U.R Singh, (2012), "Effect of Dusty Viscous Fluid on Unsteady Laminar Free Convection Flow Through Porous Medium along a Moving Porous Hot Vertical with Thermal Diffusion." Applied Mathematical science. 6,6109- 6124.

[4] Andrea Diani, Kartik K. Bodla, Luisa Rossetto, Suresh V. Garimella, "Numerical Analysis of Air Flow Through Metal Foams." Science Direct, Energy Procedia 45 (2014) 645-652, 68th Conference of the Italian Thermal Machines Engineering Association, ATI2013, Elsevier.

[5] Simone Mancin, Claudio Zilio, Andrea Diani, Luisa Rossetto, "Experimental Air Heat Transfer and Pressure Drop Through Copper Foams." Experimental Thermal and Fluid Science 36 (2012) 224-232, Elsevier.

[6] Koltsakis, G., Katsaounis, D., Samaras, Z., Naumann, D. et al., "Filtration and Regeneration

Performance of a Catalyzed Metal Foam Particulate Filter.", SAE International, Technical Paper 2006-01-1524.

[7] Rémy Ghidossi, Jean-Philippe Bonnet, Georgette Rebollar-Perez, Emilie Carretier, Jean-Henry Ferrasse, Jérôme Vicente, Frédéric Topin, Philippe Moulin, "Separation of Particles from Hot Gases Using Metallic Foams", Journal of Materials Processing Technology 209 (2009) 3859–3868.

[8] Nawaz, Kashif; Bock, Jessica; and Jacobi, Anthony M., "Thermal-Hydraulic Performance of Metal Foam Heat Exchangers.", International Refrigeration and Air Conditioning Conference, Purdue University, Purdue e-Pubs, Paper 1283, 2395, Page (1-10), 2012.

[9] D.A. Nield, A. Bejan, "Convection in Porous Media", third ed., pringerVerlag, New York, 2006.

[10] S. Whitaker. Flow in porous media i: A theoretical derivation of the Darcy's law. Transp. Porous media, 1:325, 1986.

[11] Ergun, Sabri, "Fluid Flow through Packed Columns." Chemical Engineering Progress, Vol. 48, No 2. (1952): 89-94.

[12] Vafai, K., 1986, "Analysis of the Channeling Effect in Variable Porosity Media," ASME J. Energy Resources Technology, 108, pp. 131-139.

[13] Shyamanta, "MHD flow and heat transfer of a dusty viscoelastic stratified fluid down an inclined channel in porous medium under variable viscosity", Theoretical and applied mechanics , vol.26,PP.1-14 , 1998.

[14] Al-Sumaily Gazy F , John Sheridan, Mark C. Thompson, "Analysis of forced convection heat transfer from a circular cylinder embedded in a porous medium" International Journal of Thermal Sciences 51 (2012) 121-131.

[15] Salman H. Obaid, "Laminar Forced Convection of Dusty Air through Porous Media in a Vertical Annulus", Journal of Engineering, ISSN: 17264073, Year: 2014**,** Volume: 20, Issue: 9,Pages: 90-107.

[16] M. Kaviany. Principles of Heat Transfer in Porous Media. Springer—Verlag, New York, 1991.

[17] P. Nithiarasu, K.N. Seetharamu, and T. Sundararajan. Natural convective heat transfer in an enclosure filled with fluid saturated variable porosity medium. Int. J. Heat Mass Transfer, 40:3955—3967, 1997.

[18] Wajeeh K. H. (2006) "Transient Three-Dimensional Natural Convection in Inclined Confined Porous Media". Ph.D. Thesis, University Of Technology.

دراســـة الاداء الهيدروليـكي والحـراري لمـرشح مصنـوع مـن رغـوة معدنيــة

إحسان يحيى حسين
محمد ياسين شاكر
قسم الهندسة الميكانيكية
كلية الهندسة/ جامعة بغداد
بغداد / العراق

الخلاصة:

يتضمن البحث الحالي دراسة الاداء الهيدروليكي والحراري لمرشح مصنوع من رغوة معدنية تجريبيا وعدديا لهواء نظيف ومغبر. نوعين من الكثافة المسامية (PPI) تم استخدامها في البحث , 10 مسام بالانج الواحد مع معدل قطر مسامي 905.7 µm مع مسامية (90%) و40 PPIمع معدل قطر مسامي 568.6 µm مع مسامية (89%). المرشح المصنوع من رغوة معدنية نحاسية تم تعريضه الى هواء نظيف ومغبر ذو درجات حرارة مختلفة وثابتة ولقيم مختلفة من رقم رينولدز المسامي ,(Rep) لـ 10 (119.1, 168, 218, 306.8, and 356.7) PPIولـ 40 ,104.21 ,73.8) PPI (135.21, 190.3, and 221.3). العينات اختبرت في النفق الهوائي وعرضت الى هواء نظيف ومغبر ولدرجات حرارة دخول هواء مختلفة ((29.7 (65˚C, 60˚C, 50˚C, 40˚C, كشرط حدي حراري. الاختبارات تضمنت توزيع مقاييس الضغط ودرجات الحرارة خلال النماذج المصنوعة من الرغوة المعدنية النحاسية. الحل العددي للمسألة تم فيه دراسة ومناقشة تأثير درجات الحرارة والضغط بأستخدام برنامج كومسول الاصدار 4.3 bبحل معادلات (الاستمرارية, الزخم (فورخهايمر), والطاقة) ولثلاثة ابعاد. الدراسة العددية شملت جميع حالات العمل التجريبي. اثبتت النتائج ان الضغط المطلق يتناقص على طول اتجاه الجريان, ويزداد مع زيادة رقم رينولدز المسامي. لم يلحظ تأثير لدرجة الحرارة على النتائج. اثبتت النتائج ان فرق الضغط (ΔP) للهواء النظيف خلال مرشح الرغوة المعدنية النحاسية مع PPI40أعلى بمقدار (57.8%) منه خلال 10 .PPIللهواء المغبر اثبتت النتائج ان الضغط المطلق يزداد بزيادة تركيز الغبار (C) او زيادة كثافة الغبار ,(N= 2, 4, 6 & 8) وان فرق الضغط (ΔP) للهواء المغبر خلال مرشح الرغوة المعدنية مع PPI40أعلى بمقدار (58.09%) منه خلال 10 ,PPIوان فرق الضغط للهواء المغبر بكثافة غبار (N= 2 & 4)اعلى بمقدار (33%) منه للهواء النظيف ولنفس الظروف. تم أجراء مقارنة بين الدراسه العملية والنظريه للبحث الحالي, والمقارنة اثبتت تشابه السلوك مع اصغر واكبر انحراف 1-5%)). النتائج التجريبية والعددية المعروضة كذلك تم مقارنتها مع الدراسات السابقة المتوفرة للضغط مع اتجاة جريان الهواء (x-axis) و فرق الضغط التدريجي (ΔP/L)مع السرعة , واعطت نتائج مرضية.

<u>الكلمات الرئيسية</u>: مرشح مصنوع من الرغوة المعدنية, الهواء النظيف والمغبر, دراسة عددية وعملية